Faculteit Bètawetenschappen

Physics and Astronomy

Bachelor Thesis

Analysis of FoCal performance for multiple orientations using cosmic muons

Author:
Davey Oogjes
Student ID: 4021061

Supervisors:
Prof. Dr. T. Peitzmann
Subatomic Physics
Dr. Ir. G.J. Nooren
NikHef

June 14, 2017

Utrecht University

Abstract

The topic of this research is the Forward Calorimeter(FoCal) prototype. To tune this detector, cosmic muons were used, but with the detector upside down, resulting in backward tracks. However, due to the presence of a tungsten block in the detector, multiple scattering effects could not be ignored. From 2016 onwards, the detector was put in the correct orientation to analyse its performance and find out whether there are any discrepancies between data taken in these two orientations.

For the found tracks in the two orientations the cluster size distribution, the angular distribution and the alignment of the sensors were not significantly different.

A new tracking algorithm was also developed to find tracks for muons that experienced multiple scattering, since this would most likely make them undetectable for the normal tracking algorithm. With this new tracker the angular distribution and the alignment of the sensors were similar to the results found using the normal tracker. The cluster size distribution was different, but this was a consequence of the principles of the new tracking algorithm.

With this new tracker, the track finding efficiency improved by 15.9% to 20.8% for the tracks taken with the detector upside down. For the tracks taken with the detector in the correct orientation this improvement was 2.1% and 5.4%.

It was also found that the detector has not been functioning correctly since it was put in the correct orientation, which explains the low track finding efficiency for the data taken with the detector in this orientation. Reasons for this have not been discovered as of yet.

Contents

1 Introduction

One of the phenomena studied in the ALICE experiment at CERN is the quark-gluon plasma. In the quark-gluon plasma, all kinds of particles are produced, pions and photons amongst others. These pions decay into photons, which makes it challenging to distinguish between direct photons and photons originating from pion decays. For this, an upgrade to ALICE was proposed called FoCal, Forward Calorimeter, a high-granularity electromagnetic digital sampling calorimeter. To find out whether this type of detector is feasible, a prototype was built and tested. Cosmic muons were used to tune the detector prototype, since these leave straight tracks in the detector. At first this was done with the detector upside down, but from 2016 onwards it was done with the detector in the correct orientation. In this research, some of the properties of the muon tracks were investigated to examine whether the orientation of the detector influenced the data.

This thesis will start by explaining the theory behind calorimeters and cosmic muons in section 2. In section 3, the FoCal prototype design will be handled, as well as the data acquisition procedure and the software and methods used. In section 4 the results of this research will be presented and finally in section 5 conclusions and possibilities for further research will be discussed.

2 Theory

Before discussing the FoCal prototype, the principles behind calorimetry need to be explained. This will be done in this section. After that multiple scattering theory for muons and lastly the mechanism behind the creation of cosmic muons will be explained.

2.1 Calorimeter principles

The goal of a calorimeter is to measure the energy of a particle. It does that by absorbing the energy of the particle and converting this energy into a usable signal. To do this every calorimeter has two sections, a section where interactions with the particle happen, called the absorber, and a section in which the energy of the particle is deposited, called the sensor. Some calorimeters are made of a material which is both an absorber and a sampler, these are called homogeneous calorimeters. The drawback of a homogeneous calorimeter is that, since it needs to be able to stop high energy particles and also convert this energy into a signal, there is a very limited amount of materials that can be used for this type of calorimeter and these materials can also be quite expensive. Calorimeters for which the absorber and sampler are separate materials are called sampling calorimeters, due to the fact that they don't continuously measure the energy, but instead sample it at certain points in the detector, generally leading to worse energy resolution. The advantage sampling calorimeters have is that a wide range of materials can be used, meaning a sampling calorimeter can be specifically designed for its function and will often be cheaper to build.

In an electromagnetic calorimeter, which is intended for electrons, positrons and photons, the high-energy particles lose their energy through what is called an electromagnetic cascade or shower. Through pair production and bremsstrahlung, they will produce new particles, which will in turn produce more particles, until the energy of the produced particles is not high enough for these interactions to occur.

An important material property is the radiation length X_0. The radiation length is the distance travelled in the material by high energy (GeV range) electrons or positrons for which they lose $1 - e^{-1}$ or 63% of their energy. The radiation length is a material property and is dependent on the density and thickness of the material. For example, for tungsten it is 3.50 mm and for silicon it is 93.7 mm.[1]

Normally, sampling calorimeters measure the energy deposited by each shower particle to reconstruct the energy of the parent particle. However, since the energy of the parent particle is divided equally over shower particles and the energy at which the shower stops is a material property, it is also possible to reconstruct the parent energy by only counting the particles produced in the shower. This is called particle counting calorimetry. Since the energy of each shower particle does not need to be known, just the amount of particles and their positions, a digital sampler would suffice.

2.2 Scintillation counters

A scintillation counter is a type of particle detector. It has two main parts, a scintillator and a photomultiplier. When a particle passes through the scintillator, it excites the electrons in the material. When these electrons drop down to their normal energy level, photons are emitted. These photons travel to the photocathode of the photomultiplier tube, where the cathode emits electrons through the photoelectric effect, which are focussed onto the first dynode. There, more electrons are produced, which are again focussed onto the next dynode and so on, amplifying the signal, until it reaches the anode of the photomultiplier, where the signal is measured. The strength of this signal is then proportional to the amount of energy deposited into the scintillator.

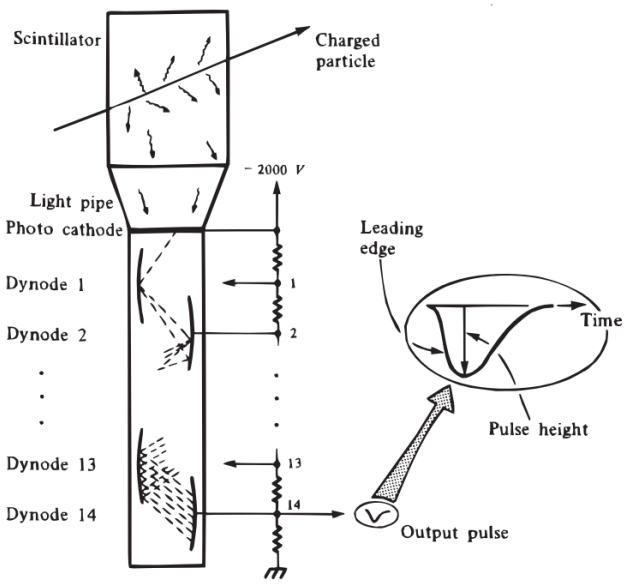

Figure 1: An example of a scintillation counter. From [2].

2.3 Multiple scattering

When charged particles travel through a medium, they can be deflected under small angles by the nuclei of the medium due to Coulomb scattering. This small angle scattering is called multiple scattering. The net scattering can be approximated by a Gaussian distribution about zero [3], where the standard deviation is given by:

$$\theta_0 = \frac{13.6 \text{ MeV}}{\beta cp} z\sqrt{x/X_0}[1 + 0.038 \ln(x/X_0)]. \tag{1}$$

In this formula p, βc and z are the momentum, velocity, and charge number of the incident particle and x/X_0 is the thickness of the scattering medium in radiation lengths. This θ_0 distribution is plotted in figure 2, for relativistic muons with $\beta \approx 1$ and for a material with a radiation length of 44 cm. This means that multiple scattering will not play a significant role for muons with energies higher than a few GeV.

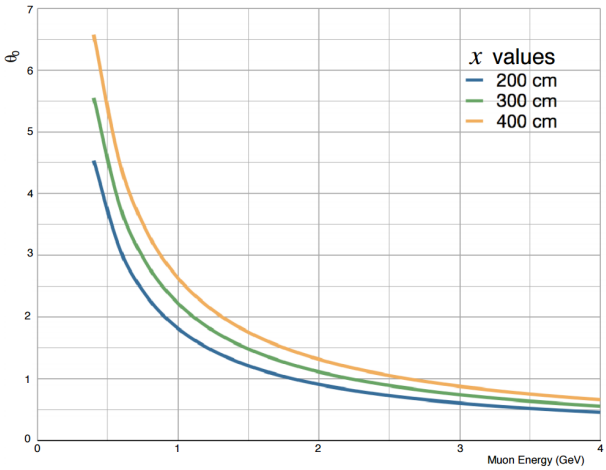

Figure 2: θ_0 distribution for relativistic muons, with $X_0 = 44$ cm and $\beta \approx 1$. From [4].

2.4 Cosmic muons

When high-energy particles from space enter our atmosphere, they might collide with a nucleus. This collision produces a cascade of particles, shown in 3, and some of these particles can be muons. The muons have a short lifetime, but due to their relativistic speed they can reach the surface of the earth, where they can be detected. As the energy of the parent particles covers a wide spectrum, so does the muon energy spectrum. This energy spectrum of cosmic muons is plotted in figure 4 and shows a spectrum ranging from 1 to over a 1000 GeV.

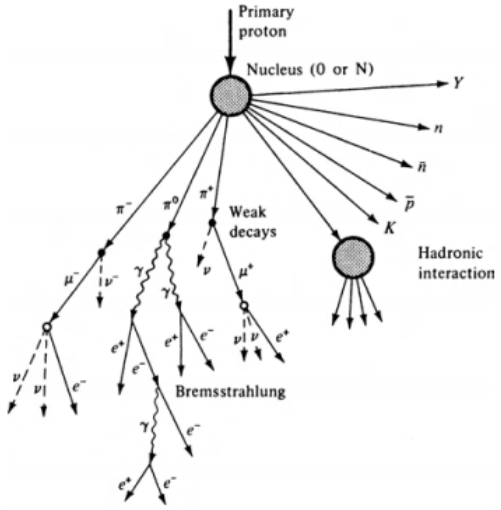

Figure 3: Incoming high-energy proton hits a nucleus at the top of the atmosphere and produces a particle cascade. From [2].

In a detector, muons generally travel in a straight line, since they do not produce a shower, unlike electrons or photons, for example. As is shown in figure 2, muons with energies above a few GeV are not strongly affected by multiple scattering, and as is shown in 4, the muons that are affected only make up a small part of the total energy spectrum, so it can be assumed that most cosmic muons will not be strongly scattered by the detector material.

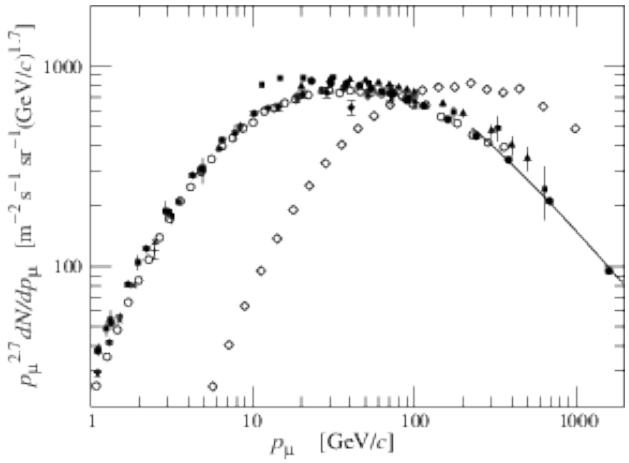

Figure 4: Energy spectrum of cosmic muons for two angles of incidence, $\theta = 0°$ (left curve) and $\theta = 70°$ (right curve). From [3].

3 Experimental setup and methods

In this section, first the FoCal prototype design will be handled. The information in this section follows [1]. After that the data acquisition procedure, the software used for data analysis and the methods of this research will be discussed.

3.1 The FoCal prototype

3.1.1 Detector geometry

FoCal, or Forward Calorimeter, is a digital sampling electromagnetic calorimeter. It consists of 24 layers, with the absorbing material being tungsten and the sampling material being digital silicon pixel sensors with a pixel size of 30×30 μm^2, giving the detector a very high position resolution. Since each sensor has a pixel surface of 640×640 pixels, the total pixel area of the sensors is 19.2×19.2 mm^2, which is quite small. To increase the surface area of the layers, each layer consists of 4 sensors, arranged 2 by 2. Since the detector is a prototype, the sensor thickness ranges from 14μm to 20 μm. The tungsten contributes a total of 3.38 mm to each layer, and together with other small contributions the total thickness of each layer is 3.97 mm, while the radiation length is 4.04 mm. This gives the layers of the prototype a combined depth of 23.4 radiation lengths. As is shown in figure 5, there is also a block of tungsten at the end of the detector. This makes the depth a total of ≈ 27 radiation lengths. This is enough to contain most of the energy of the high-energy particles that the detector is intended for. It is important to note that the particles, when they hit a pixel, tend to leak charge to neighbouring pixels, creating clusters of hits.

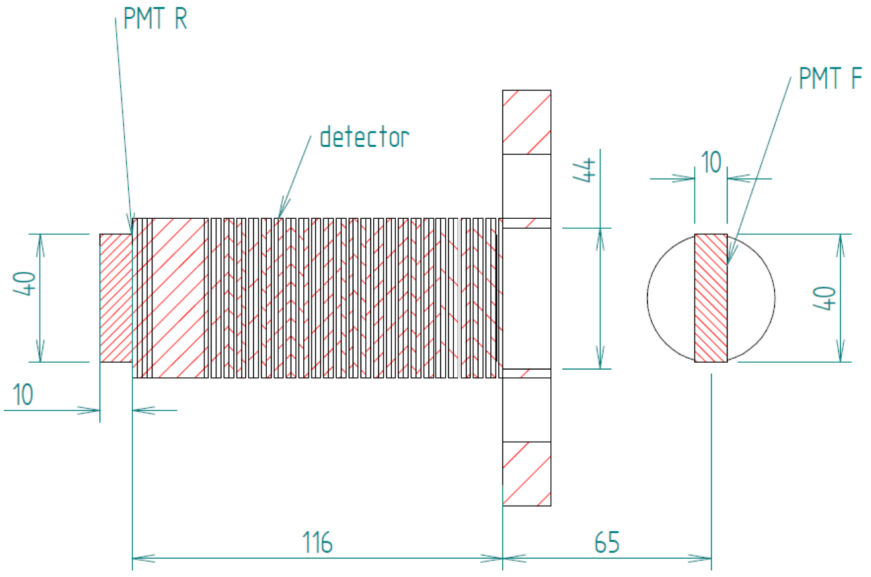

Figure 5: Side view of the FoCal prototype. The dashed blocks are tungsten and the thick lines are silicon sensor layers. PMT F and PMT R are the front and rear scintillators respectively. From [5].

3.1.2 Detector readout

The sensors used in the FoCal prototype are connected to one discriminator for each column. These columns are read out sequentially, through what is called a rolling shutter. The readout of one row of pixels takes 1 μs, meaning it takes 640 μs to read out the entire sensor. The readout of the 96 sensors of the detector is done simultaneously, meaning the readout of the detector also takes 640 μs. The data produced by the detector is not immediately usable, because 40 pixel signals are combined into one signal, and 4 of these are again combined, in a process called multiplexing.The detector is read out continuously, so there needs to be

a way to find the data for which a particle has travelled through the detector. This is done using a trigger system consisting of multiple scintillators. If the trigger system detects a particle, it sends a signal and the detector readout is saved. However, it might happen that a particle enters the detector while a readout is already underway, so the particle might hit the part of a sensor that has already been read out, leaving it undetected. To account for this, 3 readouts are saved, the readout before the trigger, the readout during which the trigger was sent and the next readout. These 3 readouts are called a frame.

3.2 Cosmic muons in FoCal

To tune the detector response, minimum ionizing particles are used. These particles will deposit a known amount of energy into the detector and will go through the detector in a mostly straight line, called a track. The particles commonly used for this, which are also used for the FoCal prototype, are cosmic muons. This section will go into the data acquisition procedure for cosmic muons and the processing of the acquired data to recreate the tracks left by the muons. After that it will go into detail about one of the uses for these tracks, namely the alignment of the silicon sensors.

3.2.1 Data acquisition for cosmic muons

When taking cosmic muon data, a trigger system consisting of two scintillators is used, one at the top and one at the bottom of the detector, PMT F and PMT R in 5 respectively. When they send coinciding signals, this indicates a particle entering and leaving the detector, which is likely to be a minimum ionizing particle, in this case a cosmic muon.

Before cosmic muon data is taken, a noise run, also called a pedestal run, needs to be done. During a pedestal run the detector collects data while ignoring the trigger system, so the background noise can be determined and corrected for. For the cosmic muons, often one frame is collected. After a pedestal run, a cosmics run is started. During this the detector is continuously taking data, often over multiple days. When the run is done, the data is demultiplexed and the background noise is corrected for using the data from the pedestal run. After this procedure, the data can be analysed and the muon tracks can be found.

3.2.2 Track finding algorithms

From the coordinates of the pixels hit in each layer, the track of the muon can be reconstructed. This is not as simple as it seems however, since not all the background noise hits can be eliminated. To find the hits that belong to the track, tracking algorithms can be used used. For this research, two tracking algorithms were used, each exploiting a different property of the muon tracks.

The first tracking algorithm, from this point on called the normal tracker, is based on the property that all hits of a track must lie along the same line. It first connects pairs of hits into what is called *tracklets*. If these tracklets do not intersect the planes on the top and bottom of the detector, they are discarded since the particle must have gone through both scintillators for the system to send a trigger. After this the region with the highest number of tracks in 1 mm is taken as the *region of interest*. The tracklet with the highest number of neighbouring tracklets in this region is then taken as the *seed* track. All hits within 1 mm of the seed track are then added to this track and if the number of hits in the track is at least 24 hits in at least 12 layers, it is saved.

The second tracking algorithm, from now on called the multiple scattering tracker, was developed to find the tracks that the normal tracker could not find because the requirements were too strict to find tracks that underwent multiple scattering, like the track shown in figure 6. It is based on the idea that the clusters of hits found when analyzing tracks are unlikely to be created by random noise. In a typical frame, there are around 400 noise hits, so in a detector with $640 \times 640 \times 96 = 39321600$ pixels, the chance of 2 or more adjacent hits being due to noise is very small.

The algorithm first calculates a straight line fit through the found clusters if there is a minimum of 5 clusters, each in a different layer. Clusters with more than 10 hits are discarded because these are likely due to faulty sensor areas. After this, the influence of each cluster on the fit is estimated, using *Cook's Distance*. This is defined as:

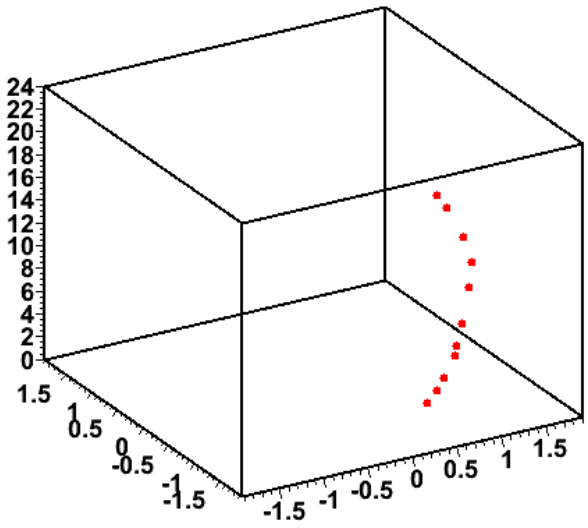

Figure 6: Example of a curved track, found in run 967.

$$D_i = \frac{e_i^2}{s^2 p}[\frac{h_i}{(1-h_i)^2}] \tag{2}$$

where D_i is the Cook's Distance for the i-th cluster, e_i is its residual value, the difference between the observed position of the center of the cluster and the intercept of the straight line fit with that sensor, n is the amount of clusters in the potential track, p is the amount of fit parameters, s^2 is the mean squared error, defined as:

$$s^2 = \sum_{i=1}^{n} \frac{{e_i}^2}{n-p} \tag{3}$$

and h_i is the leverage, defined as:

$$h_i = \frac{(x_i - \bar{x})^2}{\sum_{j=1}^{n}(x_j - \bar{x})^2} + \frac{1}{n} \tag{4}$$

where $\bar{x}$ is the mean position of all the clusters in the potential track. This is done separately for both coordinates, after which the total Cook's Distance is calculated with $D_{i,tot} = \sqrt{D_{i,x}^2 + D_{i,y}^2}$. When the total Cook's Distance of the cluster is higher than $\frac{4}{n-p}$ or its residual value is above 1 mm, it is discarded. If the amount of clusters after removal is 4 or higher, the track is saved.

An example of this outlier detection is shown in figure 7, with the corresponding Cook's Distance and residual values shown in table 1. In figure 7a, one of the clusters does not appear to be part of the track, but it does influence the data strongly. As can be seen in table 1, the Cook's Distance and residual values are above the threshold, hence the cluster is removed. In figure 7b, the cluster is removed and the fit appears to be more accurate.

Table 1: Table of total Cook's Distance and residual values for the biggest cluster in each layer. Layers where these values are 0 did not detect a cluster.

Layer	Total Cook's Distance	Total residual (mm)
2	1.4×10^{-4}	$2.3 * 10^{-2}$
3	3.1×10^{-5}	$8.5 * 10^{-3}$
4	9.7×10^{-6}	$2.3 * 10^{-2}$
5	9.3×10^{-5}	$2.3 * 10^{-2}$
6	0	0
7	0	0
8	6.3×10^{-4}	$5.7 * 10^{-2}$
9	0	0
10	0	0
11	0	0
12	3.3×10^{-3}	$1.2 * 10^{-1}$
13	0	0
14	0	0
15	7.0×10^{-3}	$1.6 * 10^{-1}$
16	0	0
17	44	1.1
18	0	0
19	0	0
20	0	0
21	0	0
22	0	0
23	0	0
24	1.4×10^{-1}	$3.3 * 10^{-1}$

(a) (b)

Figure 7: An example of outlier detection. On the left a muon track with a potential outlier is shown. The straight line is a straight line fit through the data. Note that one point influences the straight line fit strongly although it appears not to belong to the track. On the right the same track is shown, after using the *Cook's Distance* method to detect the outlier and remove it.

3.2.3 Sensor alignment

Due to the high position resolution, misalignment of the sensors will have a negative effect on the quality of the data. To find this misalignment, the straight tracks from the cosmic muons can be used. The correct alignment is calculated by making a straight line fit through the hits of the track and calculating the residual. By minimizing the residuals for multiple tracks the correct alignment parameters can be found.

3.3 Methods

At first cosmic muon data was taken with the detector upside down, resulting in backward tracks. However, it was unknown whether multiple scattering due to the tungsten block could be ignored. From 2016 onwards, the detector was oriented correctly. It is important to know whether there were any discrepancies between the tracks found with the detector upside down and the detector in the correct orientation. Another thing to investigate is whether the sensors move when the detector is moved. To find this out, there are a few properties that will be researched, namely the size of clusters, the angular distribution of the tracks, the alignment and the efficiency of the tracking algorithms. To verify if the multiple scattering tracking algorithm gives the same results, the same analysis as for the normal tracker will be done and these results will be compared to each other.

3.3.1 Size of clusters

The tungsten block near the end of the detector might produce more pronounced effects of multiple scattering than the other layers of tungsten would, since it has a depth of ≈ 3.6 radiation lengths. Because of this multiple scattering the sensors could be hit under a slightly bigger angle, which could result in bigger clusters. Since in the upside down configuration the tungsten block is near the top of the detector, this could mean that these muons have a more bent path than the muons travelling through the detector in the correct orientation, resulting in bigger clusters.

3.3.2 Angular distribution

For the same reason, the angular distribution might show some discrepancies. For the upside down orientation, the tungsten block could bend the track of the muons, making it possible for them to exit the detector at a wider angle. However, in the correct orientation, the tungsten block is at the bottom of the detector, which could produce an even wider angle.

3.3.3 Alignment

To test whether the sensors positions are stable when the detector is moved, an alignment for both orientations can be made. If these correlate, that means the sensors are stable during transport, and also that the data from both orientations is suitable for tuning the detector.

3.3.4 Tracker efficiency

Due to the possible effects of multiple scattering and the strictness of the normal tracker, a lot of tracks might be discarded. To see if this is the case, the efficiency, meaning the percentage of tracks found for the triggers in each run, can be calculated for both trackers. This is expected to be a lot higher for the multiple scattering tracker.

4 Experimental results

4.1 FoCal performance in multiple orientations

To find out whether changing the orientation of the FoCal prototype had any effect on the tracks produced by cosmic muons and on senr alignment, me properties of the tracks were investigated, starting with the amount of hits in the clusters.
Note that runs 967-975 have the detector upside down and runs 1013-1020 have the detector oriented correctly.

4.1.1 Size of clusters

To see whether the muons produced bigger clusters due to the tungsten block, a histogram of the size of clusters for tracks found for both orientations was made, which is shown in figure 8. It shows that the cluster size distribution for both orientations is almost exactly the same, with most clusters containing 1 or 2 hits and clusters containing 5 or more hits being uncommon.

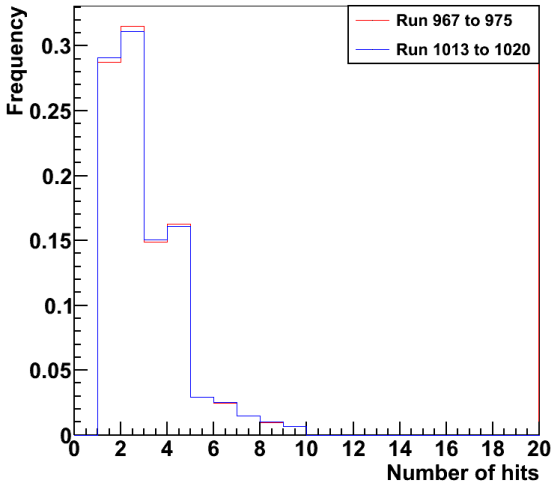

Figure 8: Comparin of the amount of hits per cluster for the tracks found for runs 967-975 and 1013-1020. Note that clusters with more than 10 hits are discarded since these are likely to be noise.

4.1.2 Angular distribution

To see whether the tungsten block had an effect on the angular distribution of both orientations, histograms were made of the angle between the hit in the first and last layer of the detector. These are shown in figure 9. They show that in both orientations the angular distribution is centered around an angle of $0°$, with angles ranging from $-12°$ to $12°$.

4.1.3 Alignment

The residuals after alignment for both orientations were computed and the correlation between these alignments is plotted in figure 10. This figure shows deviations of the order of a few μm, which is very small compared to the size of individual pixels, which is $30 \times 30 \mu m^2$.

4.2 Multiple scattering tracking algorithm

Using the multiple scattering tracking algorithm, the same analysis was done as in section 4.1 to compare it to the normal tracker. For this only runs 967-975 were used, since these runs have higher quality data than

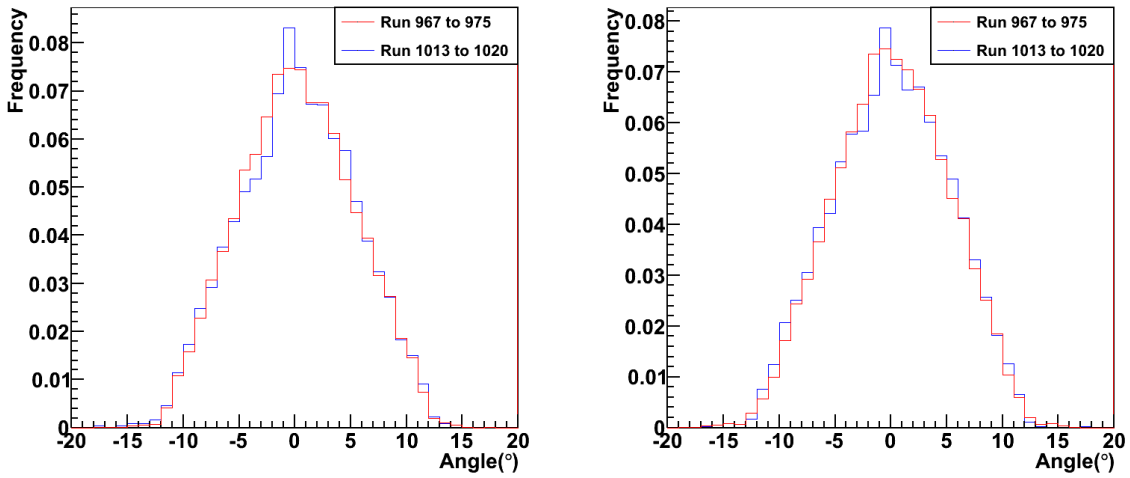

Figure 9: Normalized histograms of the angle of incidence in the x-direction(left) and y-direction(right) for all tracks of runs 967-975 and 1013-1020.

runs 1013 and 1020, as will be shown in 4.4.

4.2.1 Size of clusters

Again a histogram of the amount of hits in the clusters for tracks found using each tracking algorithm was made, which is shown in figure 11. Note that there are no clusters with one hit for the tracks found with the multiple scattering tracker, since only clusters with 2 hits or more were used. Apart from this the ratio of the frequencies of the cluster sizes has stayed the same.

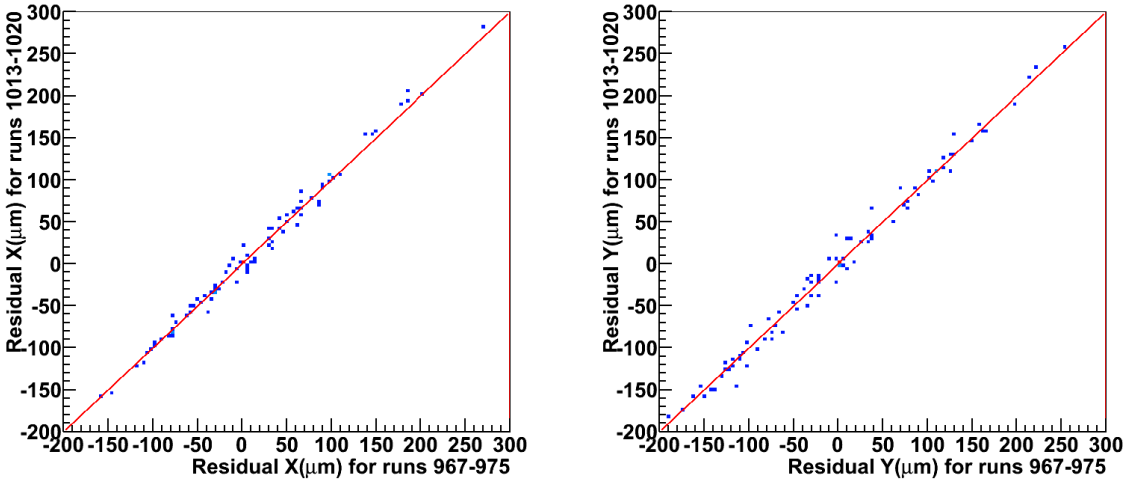

Figure 10: Correlation of residuals in the x-direction(left) and y-direction(right) for runs 967-975 and 1013-1020.

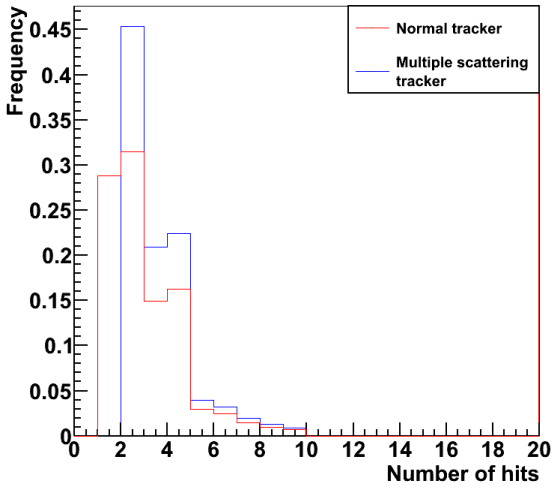

Figure 11: Comparin of the amount of hits per cluster for the tracks found for the normal tracker and the multiple scattering tracker for runs 967-975.

4.2.2 Angular distribution

The angular distribution for runs 967-975 was again calculated using both tracking algorithms. The results are shown in figure 12. Since the multiple scattering tracker is able to find more curved tracks, this distribution might have been a bit wider but this is not the case. This is not strange though, since the muons need to travel through the bottom scintillator for the detector to be triggered, limiting the angular distribution.

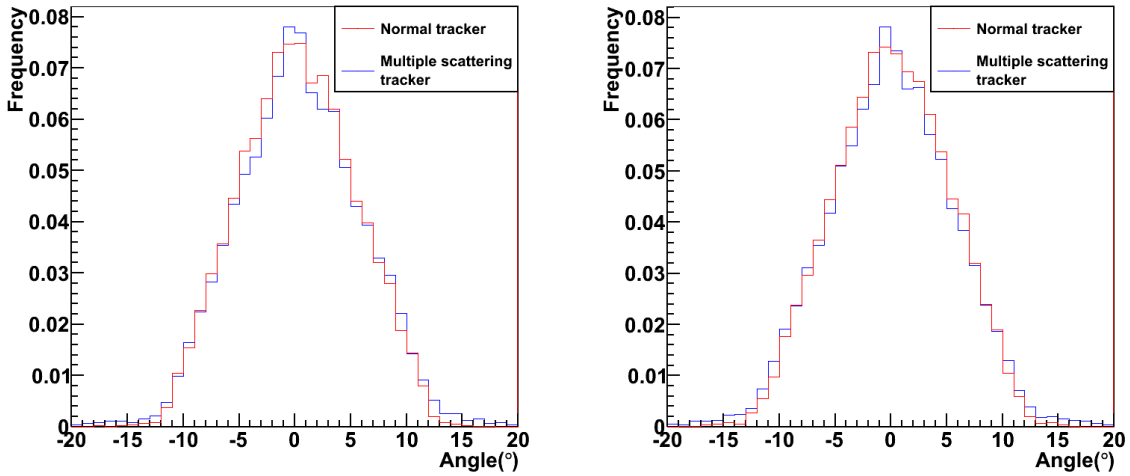

Figure 12: Normalized histograms of the angle of incidence in the x-direction(left) and y-direction(right) for tracks found with the normal tracker and the multiple scattering tracker for runs 967-975.

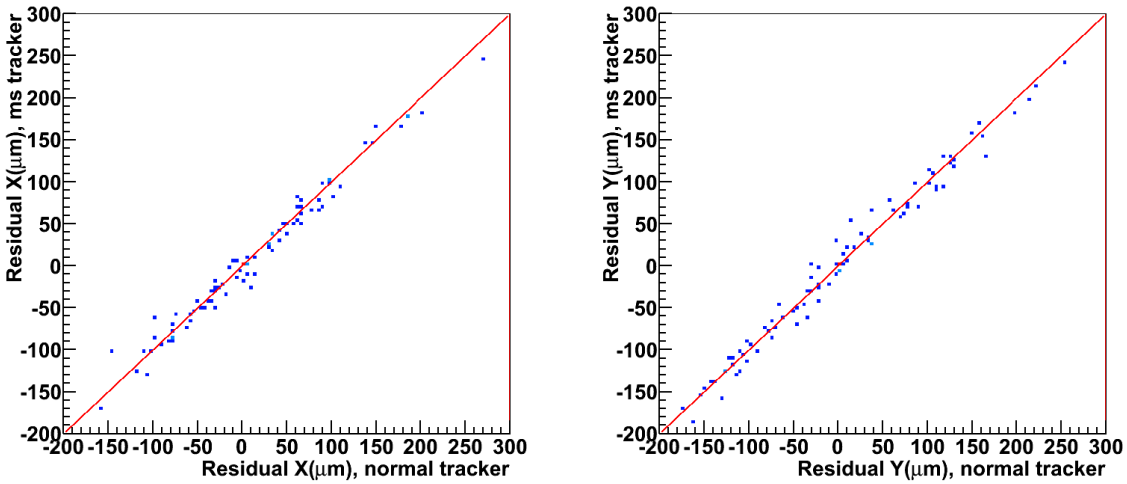

Figure 13: Correlation of residuals in the x-direction(left) and y-direction(right) for tracks found using the normal tracker and the multiple scattering tracker for runs 967-975.

4.2.3 Alignment

To be certain the tracks found using the multiple scattering tracker were correct, an alignment was made again and this was compared to the alignment made using the normal tracking algorithm. This is plotted in figure 13. This figure, just like figure 10, shows deviations of the order of a few μm, which is very small compared to the size of individual pixels, which is $30 \times 30 \mu m^2$. It has to be noted that the aligning algorithm only takes the very straight tracks, which means the curved tracks get discarded, meaning they can not influence the alignment.

4.3 Tracker efficiency

Table 2: Table of the track finding efficiency for the normal tracking algorithm and the multiple scattering tracking algorithm.

Run	Triggers	Normal tracker (# of tracks)	Efficiency (%)	Multiple scattering tracker(# of tracks)	Efficiency (%)	Improvement (%)
967	1175	741	63.1	981	83.5	20.4
968	4886	2751	56.3	3530	72.2	15.9
969	1689	1102	65.2	1446	85.6	20.4
970	1876	1159	61.2	1539	82	20.8
971	1304	846	64.9	1102	84.5	19.6
972	1567	1000	63.8	1324	84.5	20.7
973	1837	1190	64.8	1534	83.5	18.7
974	1674	1087	64.9	1425	85.1	20.2
975	2347	1497	63.8	1944	82.8	19
1013	4140	2396	57.9	2485	60	2.1
1020	4664	2343	50.2	2594	55.6	5.4

The effiency for both trackers was calculated for both sets of runs. This is shown in table 2. The efficiency for runs 967-975 using the normal tracker is around 60%, which is quite low, since every trigger is supposed to be caused by a muon entering and leaving the detector. For these runs, the multiple scattering tracker shows

an improvement in efficiency of 15.9% to 20.7%. Note that the efficiency for run 968 seems to be lower than the efficiency for the other runs between 967 and 975. For runs 1013 and 1020 the normal tracker efficiency and the improvement in efficiency with the multiple scattering tracker is much lower than it is for the runs in the upside down configuration. The rean for this is outlined in the following section.

4.4 Detector stability

In the previous section, the efficiency was calculated for both tracking algorithms. For runs 1013 and 1020, the efficiency for each tracker is noticeably lower than it is for the other runs. To find if there was anything wrong with the data, a hitmap was made of all layers for each run, these are shown in figures 14 to 17 and figures 18 to 21 respectively. In both runs, more in run 1020 than in run 1013, there appear to be hot lines and hot areas that should have been masked by the pedestal run done before the data taking.

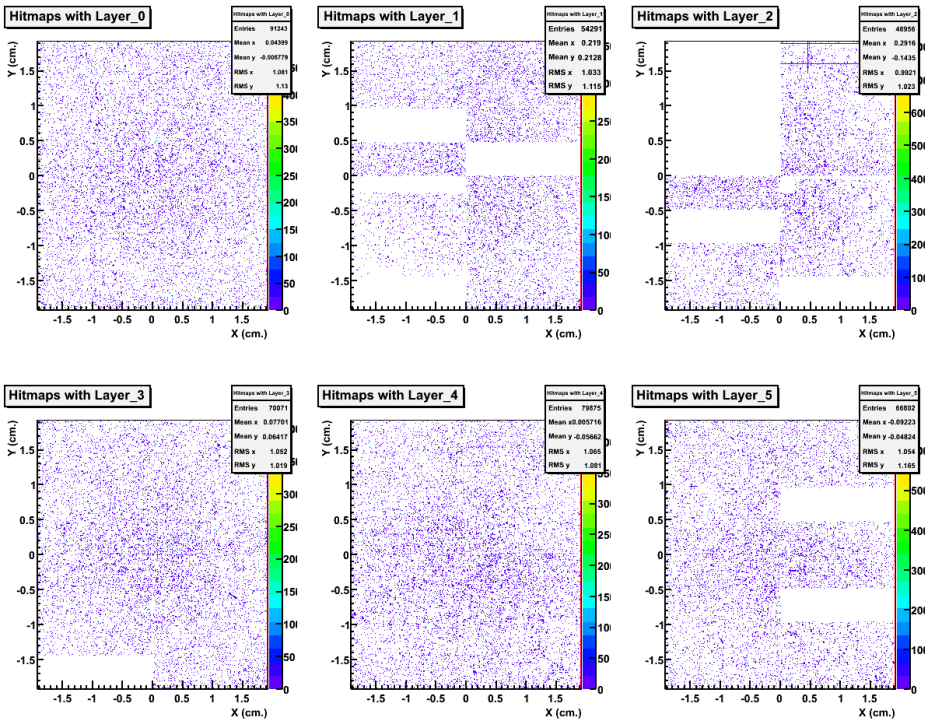

Figure 14: Hitmap for run 1013, layers 0-5.

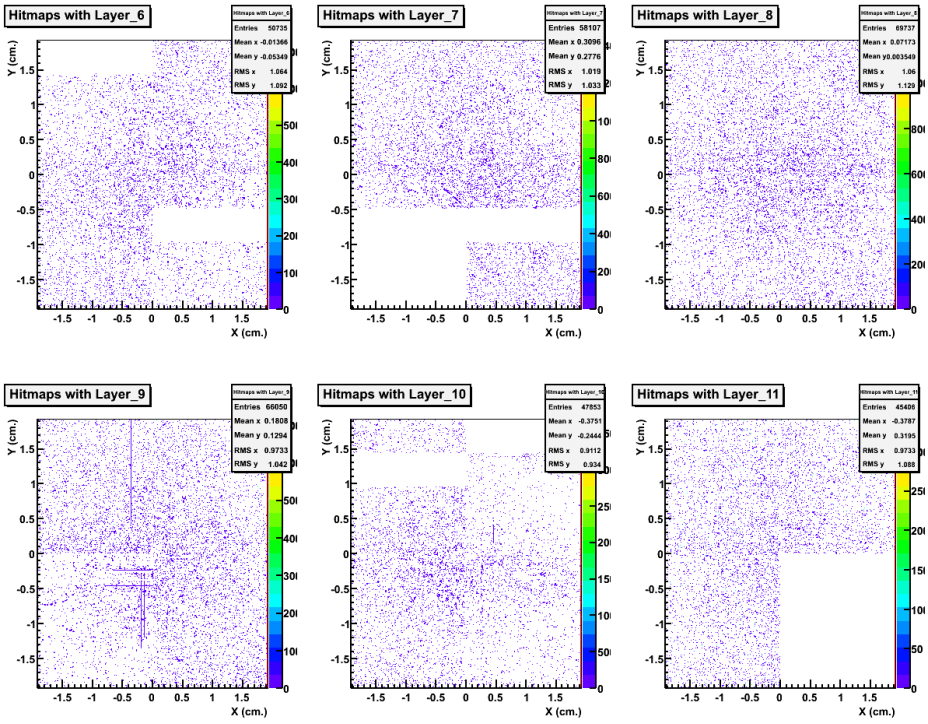

Figure 15: Hitmap for run 1013, layers 6-11.

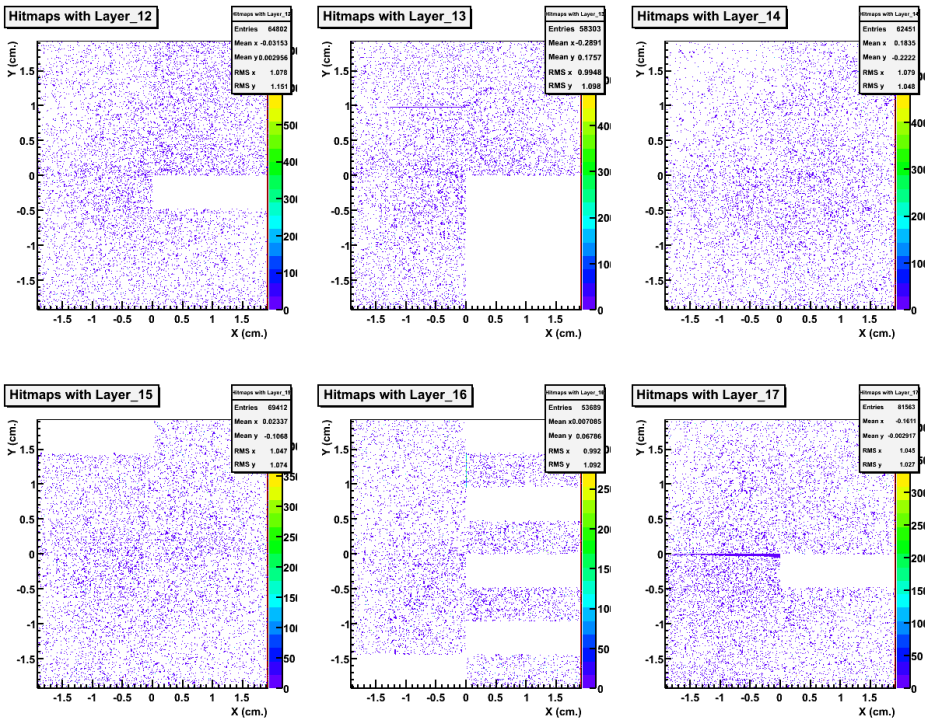

Figure 16: Hitmap for run 1013, layers 12-17.

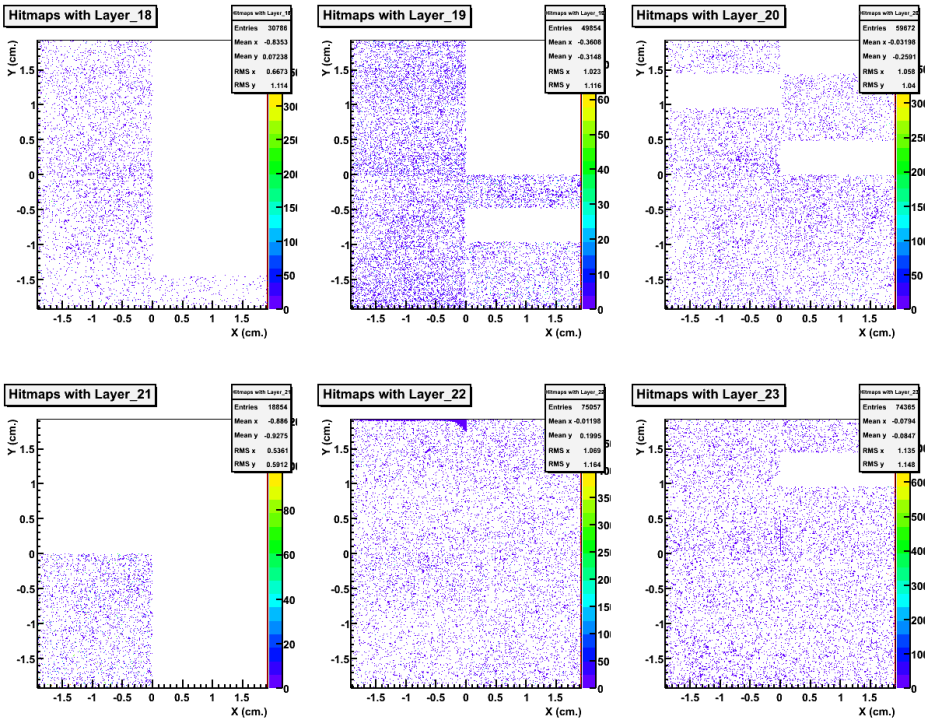

Figure 17: Hitmap for run 1013, layers 18-23.

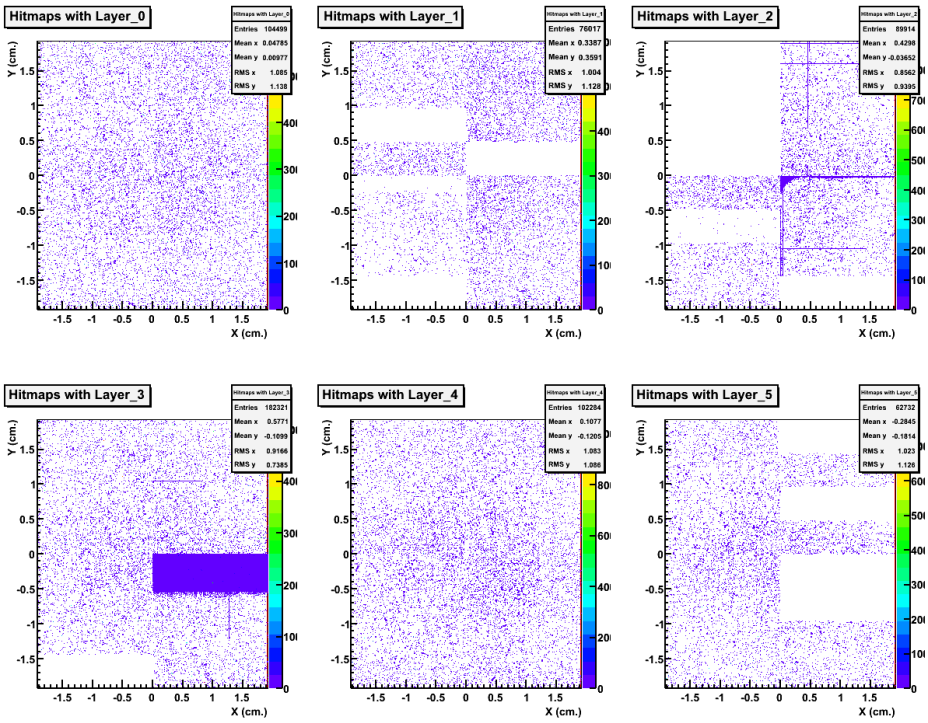

Figure 18: Hitmap for run 1020, layers 0-5.

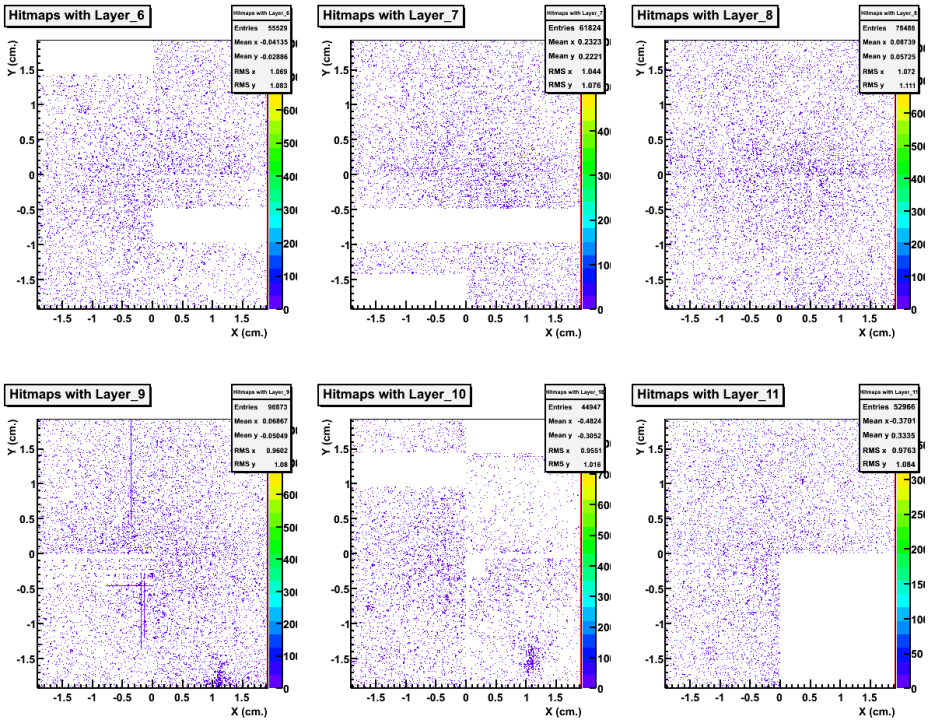

Figure 19: Hitmap for run 1020, layers 6-11.

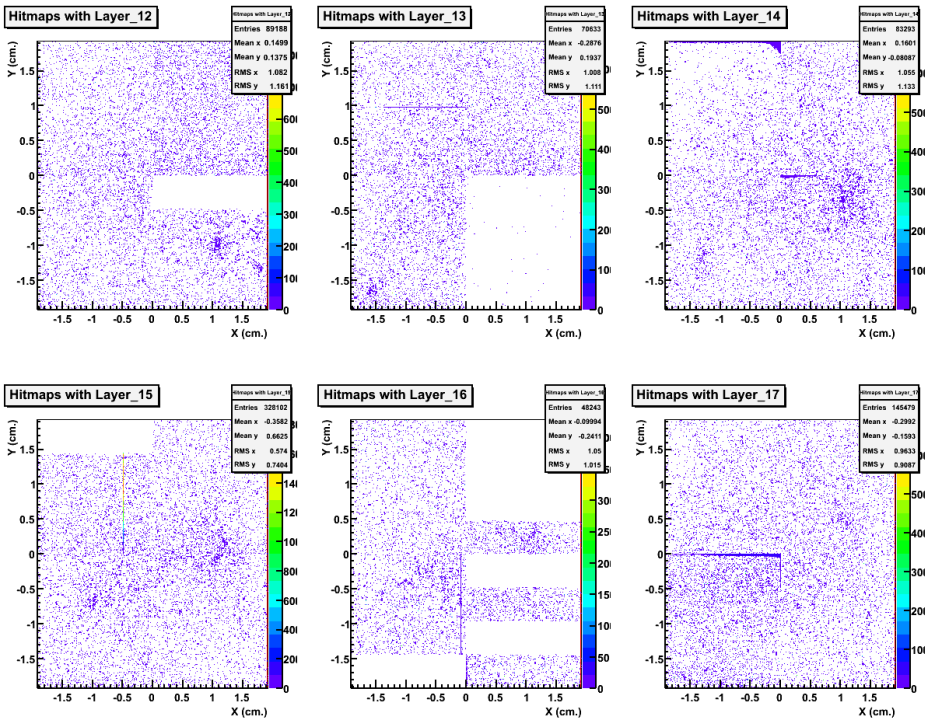

Figure 20: Hitmap for run 1020, layers 12-17.

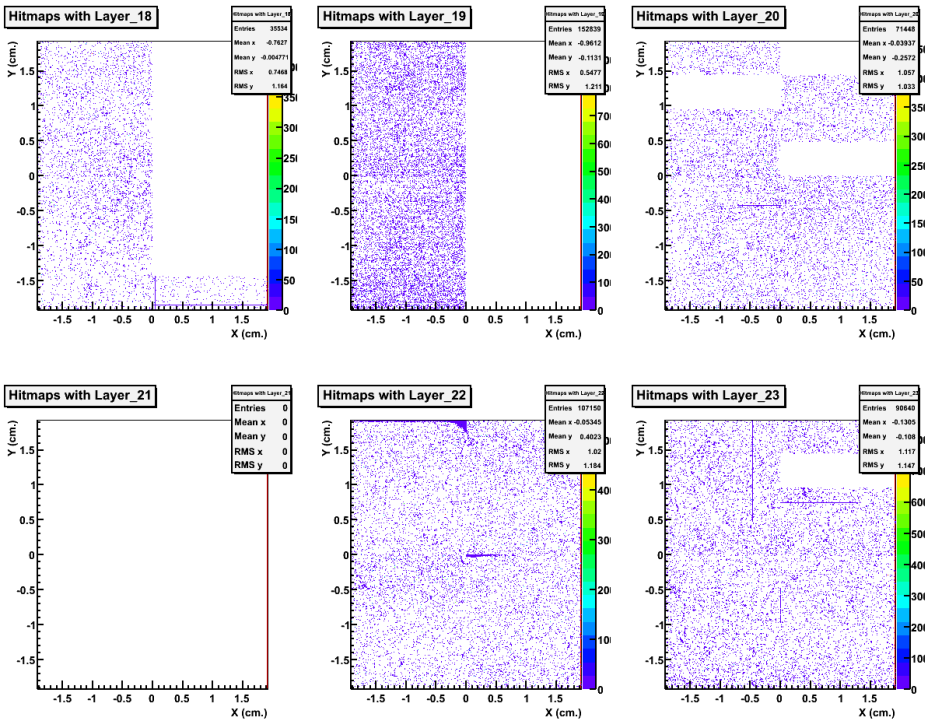

Figure 21: Hitmap for run 1020, layers 18-23.

To see whether the pedestal runs were working as intended or if the detector was malfunctioning, hitmaps were made of me of the pedestal runs. A working pedestal run, run 1027, is shown in figure 22. The pedestal run for run 1036, shown in figure 23, illustrates a problem which had not occurred before the detector was put in the correct orientation. In most senrs there appear to be hot pixels, but these are not in a line nor are they completely random, which is strange behaviour. After finding this, the detector and all the needed electronics were completely reset. The first pedestal run after the reset was correct, hence a normal data taking run was started, but during this run there were again problems, which can be seen in figure 24.

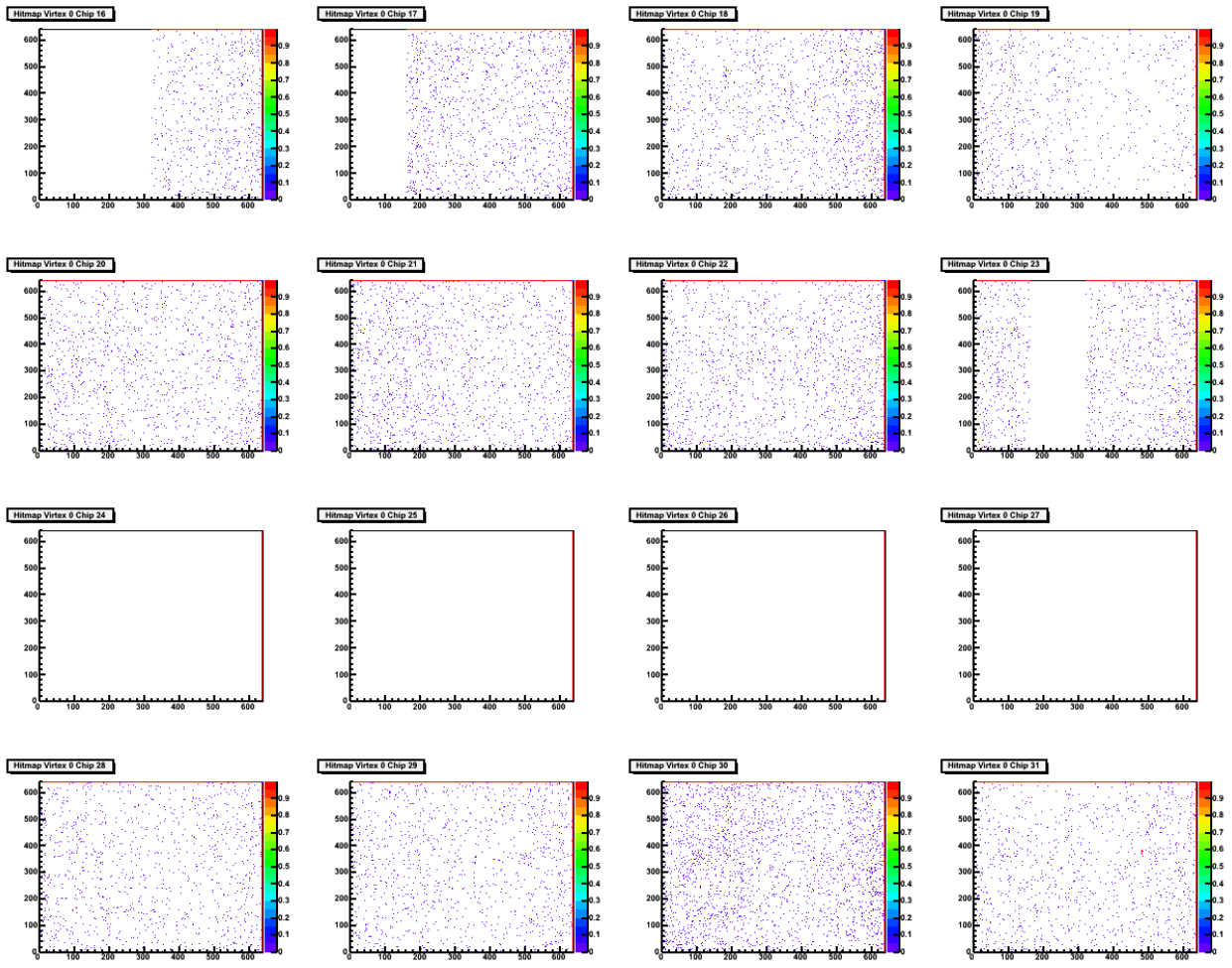

Figure 22: Pedestal hitmap for run 1027, senrs 16-31. Senrs 24-27 are dead senrs.

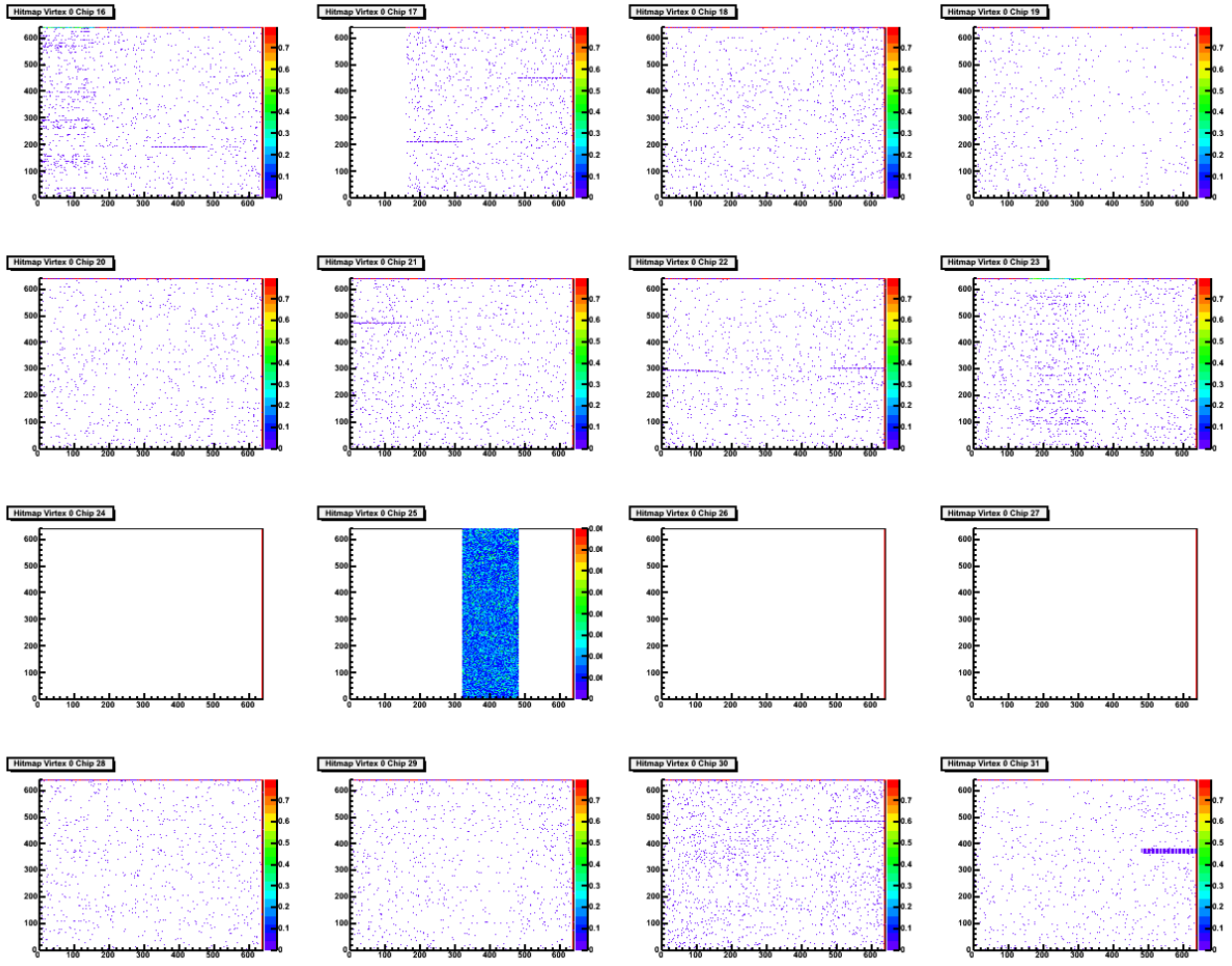

Figure 23: Pedestal hitmap for run 1036, senrs 16-31. Senrs 24-27 are supposed to be dead senrs

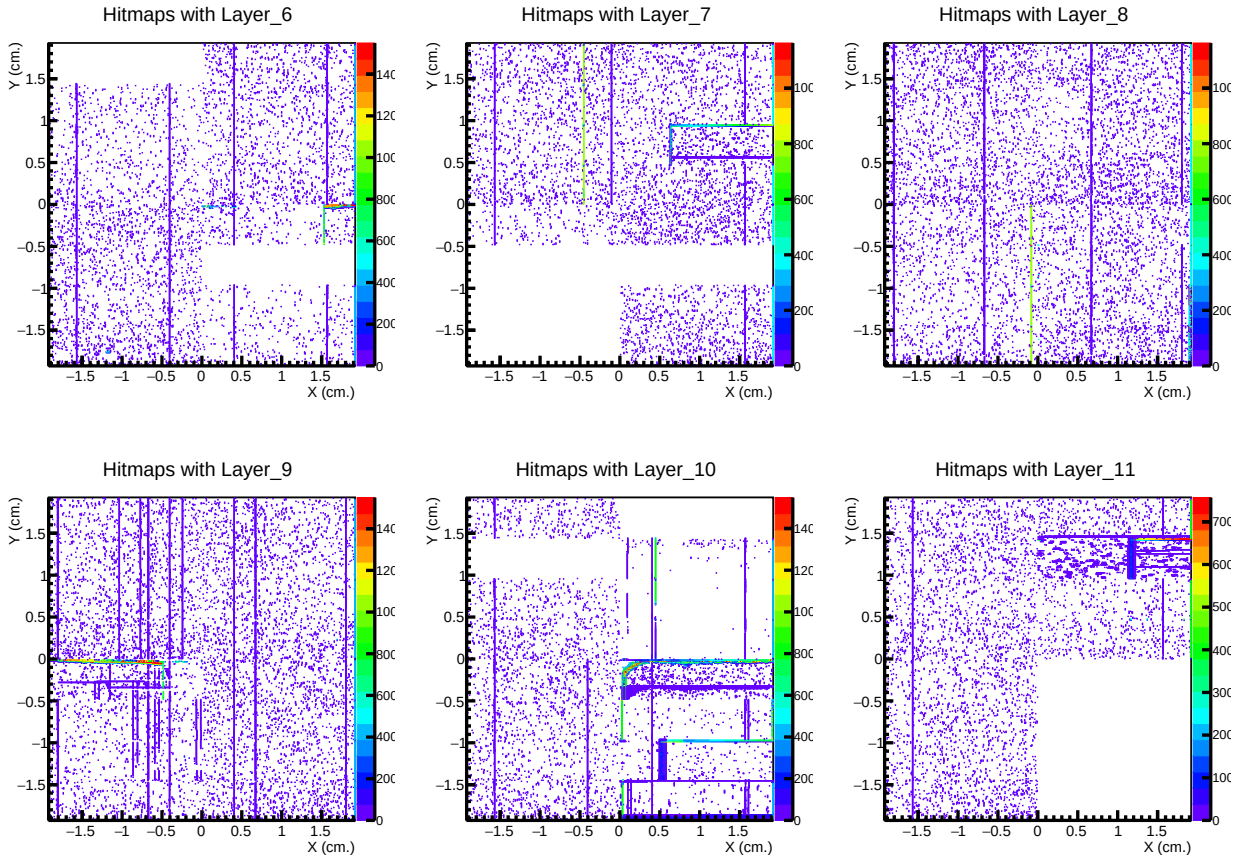

Figure 24: Hitmap for run 1054, layer 6-11.

5 Conclusions, discussion and outlook

This chapter will summarize the findings from the previous chapters and draw conclusions about these findings. Afterwards it will discuss the possibilities for further research.

5.1 Conclusions and discussion

FoCal performance in both orientations

The size of clusters, angular distribution and alignment did not change when the detector was oriented correctly. Hence it can be concluded that for the quality of the tracks, it does not matter which way the FoCal detector is oriented. This is not completely unexpected however, since the muons that would experience significant scattering would never exit the detector through the bottom scintillator, therefore a trigger would not be sent, leaving the particle undetected.

Multiple scattering tracking algorithm

The angular distribution and alignment did not change for the tracks found with the multiple scattering tracker. From this it can be concluded that the multiple scattering tracker works as intended. For the alignment it has to be noted that the aligning algorithm only takes the extremely straight tracks, which means the curved tracks get discarded, hence they do not influence the alignment. The cluster size distribution however did change. This is not strange, since clusters of one hit are no longer used to make tracks. For the other cluster sizes the shape of the histogram stayed the same. This means that multiple scattering does not play a significant role for the amount of hits in a cluster. The multiple scattering tracker significantly increased the efficiency for runs 967-975, with improvements ranging from 15.9% to 20.7%. Much higher efficiency than this can not be reached, since empty frames also occur. For runs 1013 and 1020 the improvement is significantly lower. This is most likely due to the unmasked hotlines and hotpixels. For this a mask could be made to increase the amount of tracks that can be found.

Detector stability

As was shown in section 4.4, ever since the orientation of the detector was changed, there have been problems with the performance of the detector, that were not solved by resetting the entire system. Since the software used for analysis was unchanged, it is not likely for this to be a software issue, though as of yet it is unsure what the cause of the issue is. This has to be investigated further.

5.2 Outlook

In the future, the first thing that has to be done is to find what is causing the malfunctioning of the detector. When it behaves correctly again, the calculation of the tracker efficiency for the correct orientation can be redone, to see whether it is on the same level as it was for the upside down configuration. Another thing to look into is the apparent lower efficiency for run 968. While other runs from run 967 to 975 have a tracker efficiency of 61.2% or higher using the normal tracker, run 968 has an efficiency of 56.2%. Since the amount of triggers for this run is 4886, which is over two times higher than that of the other runs, this might indicate an issue with detector stability for longer runs. This has to be investigated further. A possible use for the multiple scattering tracker is tuning the sensor response. Using the tracks found, the cluster size distribution of each individual sensor can be calculated. In theory these distributions should be the same, therefore by changing the sensitivities of the individual sensors until these distributions are the same the sensor response can be tuned.

References

[1] M. Reicher, *Digital calorimetry using pixel sensors* (2016), Ph.D. thesis.

[2] E. M. Henley and A. Garci, *Subatomic Physics* (World Scientific Publishing, 2007), 3rd ed., ISBN 978-981-270-056-8.

[3] C. Patrignani. et al (Particle Data Group), *Review of Particle Physics*, vol. C40 (2016).

[4] S. F. P. Olmedo, *Muon Energy Reconstruction Through the Multiple Scattering Method in the NOνA Detectors* (2013), Master's thesis.

[5] N. Deelen, *Tuning the focal prototype detector with cosmic muons* (2013), Bachelor's thesis.